25th IMEKO TC4 International Symposium
23rd International Workshop on ADC and DAC Modelling and Testing
IMEKO TC-4 2022
Brescia, Italy / September 12-14, 2022

Design and test of an inkjet-printed microwave interdigital capacitor on flexible Kapton substrate

Giovanni Gugliandolo[1], Andrea Alimenti[2], Kostiantyn Torokhtii[2], Nicola Pompeo[2], Giuseppe Campobello[1], Giovanni Crupi[3], Enrico Silva[2], Nicola Donato[1]

[1]*Dept. of Engineering, University of Messina, Contrada Di Dio, 98166 Sant'Agata, Messina, Italy*
[2]*Dept. of Industrial, Electronic and Mechanical Engineering, Roma Tre University, Via Vito Volterra 62, 00146, Roma, Italy*
[3]*Dept. of Biomedical and Dental Sciences and Morphofunctional Imaging, University of Messina, 98125 Messina, Italy*

***Abstract* – The inkjet printing for flexible electronics is an emerging technology that is continuously expanding in different fields, such as healthcare, sports, space science, and, in general, where the traditional rigid electronics is not adequate. In this paper, the design and test of an inkjet-printed device on a flexible substrate are presented. The device is an interdigital capacitor (IDC) fabricated by deposition of conductive ink on a 127 μm-thick polyimide (Kapton®) film. First, the electrical characterization of the substrate material is presented. The obtained results are then used for the IDC design. Finally, the prototype is fabricated by means of an inkjet printer and tested in a frequency range from 1 GHz to 5 GHz.**

I. INTRODUCTION

Recently, growing attention has been paid to inkjet printing (IJP) technology for electronics applications. The prominent factors that are playing a major role in raising the research interest in this technology include cost efficiency, fast prototyping, better optimization in large-scale production, and rapid testing of the products [1]. Moreover, such technology represents an environmentally friendly alternative to the more conventional printed circuit board (PCB) fabrication processes; the pattern is directly printed onto substrates without employing screens or masks, thus generating nearly zero waste [1].

IJP technology has witnessed a remarkable progress by moving from the design and integration of simple electronic elements (e.g., sensors [2]) to the development of more advanced systems [3]. Nevertheless, the use of inkjet printing techniques in the RF and microwave field is still limited because of the limited accuracy and repeatability of the printed patterns [4]. Furthermore, in microwave applications, an accurate control of the ink surface roughness [5] and the final ink conductivity is mandatory [6]. Despite this, the IJP technology is expected to advance significantly, as continuous innovations are being made to address these limitations and make it viable for RF and microwave device fabrication.

In such a context, many typologies of inkjet-printed microwave sensors have been proposed in the literature. In [6], a low-cost and lightweight wireless sensor node has been proposed. It includes a carbon-nanotube-based sensitive element combined with an inkjet-printed patch antenna. The developed prototype has been successfully used for ammonia detection. More recently, in [7] a chipless RFID inkjet printed humidity sensors was proposed. This prototype is composed of three concentric rings that produce three dips in the amplitude of the reflection coefficient of the microwave device. The resonant frequency of such dips was exploited as a tracker for humidity detection.

One of the biggest advantages of the IJP technology relies on the possibility to use thin and flexible/stretchable materials as substrate [8]. This allows the development of wearable devices with a higher level of wearing comfort in comparison to traditional electronics. They can be placed in contact with the human skin or integrated into clothes for different applications aimed at health care, sports, biomonitoring, and human-machine interaction [8, 9]. In such a context, several microwave devices have been proposed [9], such as flexible antennas [1], gas sensors [10], humidity and temperature sensors [11], and even more complex microwave systems have been developed for energy-harvesting [12], smart skin [13], and telecommunication applications [14].

In this paper, a preliminary design of a flexible inkjet printed microwave resonator is presented. The microwave resonator is an interdigital capacitor (IDC). This type of capacitor is used to realize small capacitances in microwave integrated circuits [15] and it is widely employed in sensing applications [16–19]. It can be modeled as a RLC series circuit [20] where R and L are the parasitic resistive and inductive elements, while C is the IDC equivalent capacitance which describes the capacitive contribution of the multi-finger structure. Similarly to RLC circuits, IDCs have a specific resonant frequency [16, 20]. The IDC design is carried out using a computer-aided de-

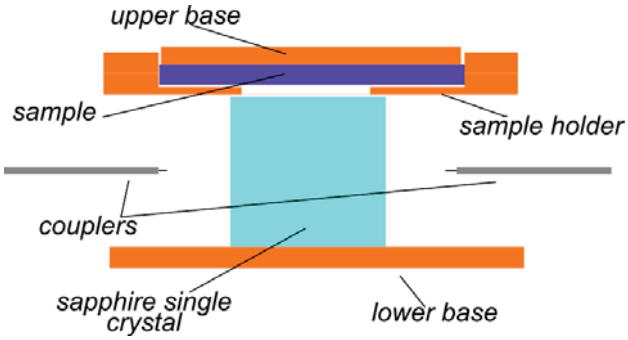

Fig. 1. Sketch of the dielectric loaded resonator used for the ε measurement of the Kapton® film. The lower/upper bases and the sample holder are made of brass. The dielectric crystal is a sapphire cylinder 5 mm high and 8 mm in diameter. The TE_{011} mode is excited through coaxial cables ended with magnetic loops at $\sim$ 12.5 GHz. The dielectric sample is loaded under the upper base and the resonator closed by applying a 500 g weight on it. Further details can be found in [24].

sign (CAD) software and validated through computer simulations. The final prototype is then fabricated on a 127-μm thick Kapton® film substrate using a Voltera V-One PCB printing machine. Tests are carried out in the frequency range spanning from 1 GHz up to 5 GHz.

The paper is organized as follows. In the next section, the electrical characterization of the flexible material used as a substrate for the microwave resonator is presented. In Section III, the design, fabrication and test of the developed prototype are discussed. Finally, conclusions are drawn in Section IV.

II. MATERIAL AND CHARACTERIZATION

The first step of the IDC design process consists in the characterization of the electromagnetic properties of the used substrate material. The values of the dielectric constant of polyimide films are rather different, depending on the source [21, 22]. Thus, a direct measure is appropriate for a suitable simulation of the device. The response of a dielectric material to electromagnetic (e.m.) fields is described through the complex dielectric permittivity $\varepsilon_0\tilde{\varepsilon} = \varepsilon_0(\varepsilon' - \mathrm{i}\varepsilon'')$, where ε_0 is the vacuum dielectric constant, $\varepsilon' = \mathrm{Re}\,\varepsilon$, $\varepsilon'' = -\mathrm{Im}\,\varepsilon$, the ratio $\tan\delta = \varepsilon''/\varepsilon'$ is known as loss tangent and $\mathrm{i} = \sqrt{-1}$ [23]. Thus, $\tilde{\varepsilon}$ of the Kapton® film used for the realization of the IDC substrate must be measured accurately to design the resonator geometry parameters. For the characterization of the Kapton® film we decided to use the dielectric loaded resonator in the configuration shown in [24] (see Fig. 1), due to its high sensitivity and precision.

The measurement method is a volume perturbation technique [25]. Part of the inner volume of an e.m. resonating structure is substituted first by a reference material and then by the material under investigation: from the variation of the quality factor Q and resonance frequency f_0, the e.m. magnetic properties of the unknown material can be estimated [25]. Air is used as reference, considering its $\tilde{\varepsilon} \approx 1 - \mathrm{i}0$. It can be shown [24, 25] that $\Delta f_0 \propto \varepsilon'$ and $\Delta(Q^{-1}) \propto \tan\delta$, where Δx is used to indicate the variation of the x parameter with respect to a reference value (of air, in this case).

Due to the expected large losses of Kapton® , only a small volume of the resonator is substituted with this material to avoid reducing too much Q and therefore losing sensitivity. The optimization of the volume of the sample, with respect to its expected e.m. properties, is discussed in [24]. In this case, to reach the desired sensitivity, ten layers of the Kapton® film are stacked to form a parallelepiped, with dimensions $15.0 \times 15.0 \times 1.27$ mm^3, and loaded into the resonator as shown in Fig. 1. To evaluate the measurement repeatability, the transmission and reflection scattering S-parameters of the resonator are measured 20 times dismounting the sample for each measurement. Q and f_0 are measured through the fit of the acquired S-parameters with the method shown in [26]. For each mounting, only one measurement was performed since it was observed that the type-A uncertainties on Q and f_0 evaluated with a statistical analysis of repeated measurements were equivalent with those provided by the fitting procedure and evaluated starting from the fit residuals of only one measurement [26].

The reference measurement is obtained substituting the same volume of the Kapton® sample with one filled with air. In this configuration the upper base of the resonator is held in position with a ring printed with the same thickness as the sample under investigation and put in the resonator in place of the sample itself. This allows not changing the geometry of the resonator but entering into the resonator a controlled volume of air. With the Kapton® sample we obtained $Q = 3866(3)$ and $f_0 = 12.45930(7)$ GHz, where the numbers in parentheses are the numerical value of the experimental standard deviations, $s(Q)$ and $s(f_0)$ respectively, referred to the corresponding last digits of the quoted results. The repetition of 20 measurements with the air reference sample gave $Q = 5066(3)$ and $f_0 = 12.486000(22)$ GHz.

The obtained Δf_0 is compared with the calibration curves $\varepsilon'(\Delta f_0)$ and $\eta(\Delta f_0)$, with η the sample filling factor [25], shown in Fig. 2, which are obtained with e.m. simulations of the structure [24]. Once ε' and η are determined, $\tan\delta \approx \Delta(Q^{-1})/\eta$ can be obtained [24].

For the analyzed Kapton® film we obtained $\varepsilon' = 4.0 \pm 0.5$ and $\tan\delta = (1.02 \pm 0.16) \times 10^{-2}$, which are in good agreement with literature values [21], and where the uncertainties are expanded uncertainties with 95 % level of probability evaluated propagating the

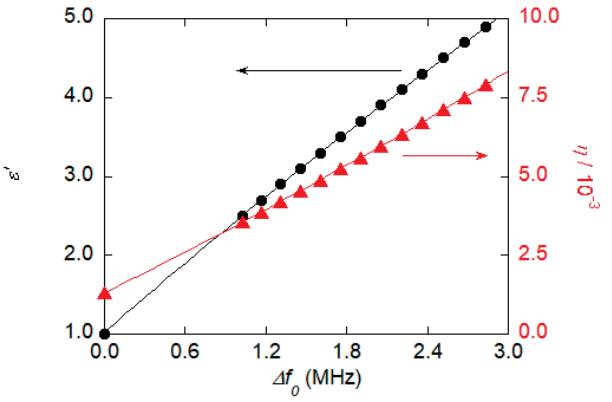

Fig. 2. Calibration curves $\varepsilon'(\Delta f_0)$ (black dots-left scale) and $\eta(\Delta f_0)$ (red triangles-right scale). The continuous curves are obtained by a 2^{nd}-order polynomial fit: $\varepsilon' = -49800(400)\Delta f_0^2 + 1512(2)\Delta f_0 + 1.000(1)$ and $\eta = 78.79(4)\Delta f_0^2 + 2.101(2)\Delta f_0 + 1.1315(2) \times 10^{-3}$, with Δf_0 expressed in MHz. The uncertainty bars are within the symbols dimensions.

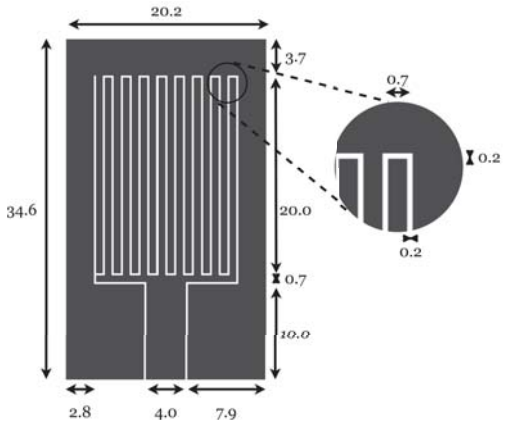

Fig. 3. Sketch of the designed one-port IDC device. All the reported dimensions are in mm.

distribution of simulated and measured quantities using a Monte Carlo method in compliance with [27, 28]. The simulated f_0 and η are assumed to be normally distributed with 1 % relative standard deviation. Thus, for each trial of the Monte Carlo simulation the calibration curves $\varepsilon'(\Delta f_0)$ and $\eta(\Delta f_0)$ are re-evaluated and fitted with a 2^{nd} order polynomial, obtaining the uncertainties on the fitting parameters reported in the caption of Fig. 2. Hence, from the measured Δf_0 and $s(f_0)$, ε' and η (and their uncertainties) are obtained, then $\tan\delta$ (and its uncertainty) is obtained from the measured Q and $s(Q)$. 10^6 trials are performed to deliver the 95 % coverage interval of the derived quantities [27].

III. DESIGN, REALIZATION AND TEST

The proposed prototype is a single-port IDC characterized by a total of 16 fingers in a parallel configuration as depicted in Figure 3. The fingers have been designed with a length, a width, and a spacing of 20 mm, 0.7 mm, and 0.2 mm, respectively. The nominal IDC dimensions are 34.6 mm × 20.2 mm. A complete description of the IDC geometrical parameters is reported in Figure 3.

The IDC geometry has been widely studied in the literature and several lumped-element equivalent circuit models have been proposed [16, 29, 30]. Such circuits accurately describe the device behavior in a relatively wide frequency range. However, at high frequency, additional resonances appear [20] and the equivalent-circuit model becomes less reliable. In this case a full-wave e.m. solver is required for the accurate study of the microwave device. As the IDC equivalent capacitance increases, spurious resonances are moved towards lower frequencies [20].

The proposed IDC is meant to be used for sensing applications and, in this case, spurious resonances are desirable since they may be exploited as trackers [31]. In the literature, IDCs and, in general, planar resonators have been employed for sensing purposes and they exhibited good performance when used in the frequency range between 1 GHz and 5 GHz [32–36]. For this reason, the proposed IDC is designed to operate on this frequency band. Several e.m. simulations are carried out on the IDC geometry. Since the IDC equivalent capacitance is proportional to the number of fingers and to their length, these two parameters are varied to get the desired result, i.e., resonances that occur in the selected frequency range. Moreover, the fingers width is chosen to maximize the quality factor of the resonant dips. The final IDC geometric dimensions are reported in Figure 3. It is worth noting that the feedline is designed with an input impedance of 50 Ω.

Once the IDC geometry is defined, the prototype is fabricated using a Voltera V-One PCB printing machine. The 127 μm-thick Kapton® film is selected as substrate, while a flexible conductive ink is used for the conductive layer printing. In particular, the Voltera Flexible Conductor 2 ink [37] is used. It is characterized by an electrical resistivity of 1.36×10^{-7} Ω·m, and the typical cured film thickness is between 40 μm and 70 μm. The prototype is printed using a 150-μm Voltera nozzle, as suggested by the ink datasheet [37], and, once the printing process is completed, the sample is cured in the oven at about 170 °C for 30 minutes. The curing procedure is essential to trigger the ink chemical reactions, thereby allowing the metal particles to fuse in a conductive layer. The IDC is then cleaned with isopropyl alcohol and burnished. Finally, a 50 Ω straight PCB mount SMA connector is soldered at the end of the feedline as an input port to allow the connection of Vector Network Analyzer (VNA).

An Agilent 8753ES VNA is used for the prototype test. The VNA is calibrated using a one-port short-open-load

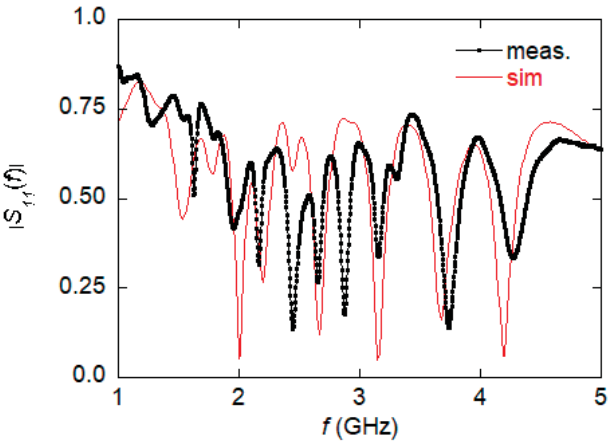

Fig. 4. Comparsion bewteen measurement (black) and COMSOL simulation (red) of the magnitude of the reflection coefficient for the developed IDC. The explored frequency range goes from 1 GHz to 5 GHz.

(SOL) calibration procedure, and the reflection coefficient S_{11} is measured. The VNA is set to acquire 1601 points, the RF power is set to 0 dBm, and the intermediate frequency (IF) is 1 kHz. In Figure 4 a comparison between the simulated and measured $|S_{11}(f)|$ is reported. As expected from simulations, several resonances occur in the considered frequency range. Simulations are carried out using the COMSOL software. A good agreement can be observed between simulation and measurement, although not all resonances are accurately predicted by COMSOL. Such mismatches may be ascribed to tolerances in the fabrication process. In particular, the fabricated prototype exhibits additional resonances in the frequency range from 2 GHz to 3 GHz. However, this should be not taken as a practical limitation for the intended applications, since the additional resonances might be exploited for detection purpose.

IV. CONCLUSIONS

In this work, the design and test of a flexible inkjet-printed IDC are presented. The design process has been supported by the electrical characterization of the dielectric Kapton® film used here as substrate. This allowed a better description of the microwave device behavior through computer simulations. The measured performance of the proposed device is found to be in line with the simulation-based expectations. Further activities are in progress in order to use the developed prototype for practical sensing applications.

REFERENCES

[1] I. I. Labiano and A. Alomainy, "Flexible inkjet-printed graphene antenna on kapton," *Flexible and Printed Electronics*, vol. 6, no. 2, 2021, Art. Id. 025010.

[2] E. Bihar, S. Wustoni, A. M. Pappa, K. N. Salama, D. Baran, and S. Inal, "A fully inkjet-printed disposable glucose sensor on paper," *npj Flexible Electronics*, vol. 2, no. 1, pp. 1–8, 2018.

[3] J. Lemarchand, N. Bridonneau, N. Battaglini, F. Carn, G. Mattana, B. Piro, S. Zrig, and V. Noel, "Challenges and prospects of inkjet printed electronics emerging applications–a chemist point of view," *Angewandte Chemie International Edition*, 2022.

[4] V. Camarchia, A. Chiolerio, M. Cotto, J. Fang, G. Ghione, P. Pandolfi, M. Pirola, R. Quaglia, and C. Ramella, "Assessment of silver nanoparticle inkjet-printed microstrip lines for rf and microwave applications," in *2013 IEEE International Wireless Symposium (IWS)*. IEEE, 2013, pp. 1–4.

[5] A. Alimenti, K. Torokhtii, N. Pompeo, and E. Silva, "Evaluation of the surface roughness detrimental effects on the surface resistance of good conductors," in *Proceedings 25th IMEKO TC4 International Symposium*. IEEE, 2022 (submitted).

[6] H. Lee, G. Shaker, K. Naishadham, X. Song, M. McKinley, B. Wagner, and M. Tentzeris, "Carbon-nanotube loaded antenna-based ammonia gas sensor," *IEEE Transactions on Microwave Theory and Techniques*, vol. 59, no. 10, pp. 2665–2673, 2011.

[7] M. Borgese, F. A. Dicandia, F. Costa, S. Genovesi, and G. Manara, "An inkjet printed chipless rfid sensor for wireless humidity monitoring," *IEEE Sensors Journal*, vol. 17, no. 15, pp. 4699–4707, 2017.

[8] K. Yan, J. Li, L. Pan, and Y. Shi, "Inkjet printing for flexible and wearable electronics," *APL Materials*, vol. 8, no. 12, 2020, Art. Id. 120705.

[9] S. Kim, "Inkjet-printed electronics on paper for rf identification (rfid) and sensing," *Electronics*, vol. 9, no. 10, p. 1636, 2020.

[10] J. George, A. Abdelghani, P. Bahoumina, E. Cloutet, N. Bernardin, K. Frigui, H. Hallil, C. Dejous, S. Bila, and D. Baillargeat, "Inkjet-printed rf gas sensors based on conductive nanomaterials for VOCs monitoring," in *2021 IEEE MTT-S International Microwave Symposium (IMS)*. IEEE, 2021, pp. 93–96.

[11] J. Courbat, Y. Kim, D. Briand, and N. De Rooij, "Inkjet printing on paper for the realization of humidity and temperature sensors," in *2011 16th International Solid-State Sensors, Actuators and Microsystems Conference*. IEEE, 2011, pp. 1356–1359.

[12] H. Saghlatoon, T. Björninen, L. Sydänheimo, M. M. Tentzeris, and L. Ukkonen, "Inkjet-printed wideband planar monopole antenna on cardboard for rf energy-harvesting applications," *IEEE Antennas and Wireless Propagation Letters*, vol. 14, pp. 325–328, 2014.

[13] M. M. Tentzeris, S. Kim, R. Vyas, A. Traille, P. Pons, H. Aubert, A. Georgiadis, and A. Col-

lado, "Inkjet-printed "zero-power" wireless sensor and power management nodes for iot and "smart skin" applications," in *2014 20th International Conference on Microwaves, Radar and Wireless Communications (MIKON)*. IEEE, 2014, pp. 1–7.

[14] L. Yang and M. M. Tentzeris, "Design and characterization of novel paper-based inkjet-printed RFID and microwave structures for telecommunication and sensing applications," in *2007 IEEE/MTT-S International Microwave Symposium*. IEEE, 2007, pp. 1633–1636.

[15] Z. A. Maricevic, "Analysis and measurements of arbitrarily shaped open microstrip structures," Ph.D. dissertation, Syracuse University, 1994.

[16] G. Crupi, X. Bao, O. J. Babarinde, D. M.-P. Schreurs, and B. Nauwelaers, "Biosensor using a one-port interdigital capacitor: A resonance-based investigation of the permittivity sensitivity for microfluidic broadband bioelectronics applications," *Electronics*, vol. 9, no. 2, p. 340, 2020.

[17] G. Gugliandolo, Z. Marinković, A. Quattrocchi, G. Crupi, and N. Donato, "Development of an inkjet-printed interdigitated device: Cad, fabrication, and testing," in *2021 IEEE International Conference on Integrated Circuits, Technologies and Applications (ICTA)*. IEEE, 2021, pp. 153–154.

[18] G. Gugliandolo, K. Naishadham, G. Crupi, and N. Donato, "Design and characterization of a microwave transducer for gas sensing applications," *Chemosensors*, vol. 10, no. 4, p. 127, 2022.

[19] Z. Marinković, G. Gugliandolo, M. Latino, G. Campobello, G. Crupi, and N. Donato, "Characterization and neural modeling of a microwave gas sensor for oxygen detection aimed at healthcare applications," *Sensors*, vol. 20, no. 24, p. 7150, 2020.

[20] F. P. Casares-Miranda, P. Otero, E. Marquez-Segura, and C. Camacho-Penalosa, "Wire bonded interdigital capacitor," *IEEE Microwave and Wireless Components Letters*, vol. 15, no. 10, pp. 700–702, 2005.

[21] S. Sahin, N. K. Nahar, and K. Sertel, "Dielectric properties of low-loss polymers for mmW and THz applications," *Journal of Infrared, Millimeter, and Terahertz Waves*, vol. 40, no. 5, pp. 557–573, 2019.

[22] S. Chisca, I. Sava, V.-E. Musteata, and M. Bruma, "Dielectric and conduction properties of polyimide films," in *CAS 2011 Proceedings (2011 International Semiconductor Conference)*, vol. 2, IEEE, 2011, pp. 253–256.

[23] J. D. Jackson, *Classical electrodynamics*. American Association of Physics Teachers, 1999.

[24] A. Alimenti, K. Torokhtii, N. Pompeo, E. Piuzzi, and E. Silva, "Characterisation of dielectric 3d-printing materials at microwave frequencies," *ACTA IMEKO*, vol. 9, no. 3, pp. 26–32, 2020.

[25] L.-F. Chen, C. Ong, C. Neo, V. Varadan, and V. K. Varadan, *Microwave electronics: measurement and materials characterization*. John Wiley & Sons, 2004.

[26] K. Torokhtii, N. Pompeo, E. Silva, and A. Alimenti, "Optimization of Q-factor and resonance frequency measurements in partially calibrated resonant systems," *Measurement: Sensors*, vol. 18, 2021, Art. Id. 100314.

[27] Joint Committee for Guides in Metrology, "JCGM 101: Evaluation of Measurement Data - Supplement 1 to the Guide to the Expression of Uncertainty in Measurement - Propagation of distributions using a Monte Carlo method," JCGM, Tech. Rep., 2008.

[28] ——, "JCGM 100: Evaluation of Measurement Data - Guide to the Expression of Uncertainty in Measurement," JCGM, Tech. Rep., 2008.

[29] G. Crupi, X. Bao, P. Barmuta, I. Ocket, D. M. M.-P. Schreurs, and B. Nauwelaers, "Microfluidic biosensor for bioengineering: High-frequency equivalent-circuit modeling of interdigital capacitor," in *2019 14th International Conference on Advanced Technologies, Systems and Services in Telecommunications (TELSIKS)*. IEEE, 2019, pp. 315–318.

[30] X. Bao, I. Ocket, J. Bao, Z. Liu, B. Puers, D. M. M.-P. Schreurs, and B. Nauwelaers, "Modeling of coplanar interdigital capacitor for microwave microfluidic application," *IEEE Transactions on Microwave Theory and Techniques*, vol. 67, no. 7, pp. 2674–2683, 2019.

[31] G. Bailly, A. Harrabi, J. Rossignol, D. Stuerga, and P. Pribetich, "Microwave gas sensing with a microstrip interdigital capacitor: Detection of nh3 with tio2 nanoparticles," *Sensors and Actuators B: Chemical*, vol. 236, pp. 554–564, 2016.

[32] L. Ali, C. Wang, F.-Y. Meng, Y.-C. Wei, X. Tan, K. K. Adhikari, and M. Zhao, "Simultaneous measurement of thickness and permittivity using microwave resonator-based planar sensor," *International Journal of RF and Microwave Computer-Aided Engineering*, vol. 31, no. 10, 2021, Art. Id. e22794.

[33] J. Bao, T. Markovic, G. Maenhout, I. Ocket, and B. Nauwelaers, "An impedance matched interdigital capacitor at 1.5 GHz for microfluidic sensing applications," *Sensors and Actuators A: Physical*, vol. 330, 2021, Art. Id. 112867.

[34] C. Wang, L. Ali, F.-Y. Meng, K. K. Adhikari, Z. L. Zhou, Y. C. Wei, D. Q. Zou, and H. Yu, "High-accuracy complex permittivity characterization of solid materials using parallel interdigital capacitor-based planar microwave sensor," *IEEE Sensors Journal*, vol. 21, no. 5, pp. 6083–6093, 2020.

[35] H.-R. Sun, G. Du, G. Liu, X. Sun, T. Tang, W. Liu, and R. Li, "Symmetric coplanar waveguide sensor loaded with interdigital capacitor for permittivity characterization," *International Journal of RF and*

Microwave Computer-Aided Engineering, vol. 30, no. 1, 2020, Art. Id. e22023.

[36] J. Yeo and J.-I. Lee, "High-sensitivity microwave sensor based on an interdigital-capacitor-shaped defected ground structure for permittivity characterization," *Sensors*, vol. 19, no. 3, p. 498, 2019.

[37] *Voltera Flexible Conductor 2 (1000383)*, Voltera, 6 2020, rev. Date 2020-06-09.